MANEUVER DETECTION VIA COMBINED HEURISTICAL AND STATISTICAL METHODOLOGIES

Guillermo Escribano[(1)], Manuel Sanjurjo-Rivo[(1)], Jan Siminski[(2)], Alejandro Pastor[(3)], and Diego Escobar[(3)]

[(1)]*Universidad Carlos III de Madrid, 28911 Leganés, , Madrid, España, Email: {guescrib, msanjurj}@ing.uc3m.es*
[(2)]*Space Debris Office, OPS-SD, 64293 Darmstadt, Germany, Email: Jan.Siminski@esa.int*
[(3)]*GMV, 28670 Tres Cantos, Madrid, Spain, Email: {apastor, descobar}@gmv.com*

ABSTRACT

Maneuver detection of Resident Space Objects is an active research topic, highly demanded in Space Surveillance and Tracking (SST) applications. The present work proposes a novel approach for tracking maneuverable objects in a reduced observability scenario. The latter is typically the case for Medium or Geostationary Earth Orbits, altitudes at which only optical observations are usually available. The novelty of the method relies on the use of a Sequential Monte Carlo framework for state estimation, enhanced by Markov Chain Monte Carlo post-maneuver state recovery. Through the definition of surrogate functions to approximate maneuvers, it is possible to recover a region of states compliant with the incoming observations provided some bounds for the maximum expected control effort. Additionally, hypotheses can be formulated based on historical data or otherwise already characterized maneuvers. Results are obtained for Geostationary spacecraft in a simulated optical observation scenario.

Keywords: Space Situational Awareness; Space Traffic Management; Maneuver Detection; Data Association; Maneuvering Target Tracking; Sequential Monte Carlo; Markov Chain Monte Carlo.

1. INTRODUCTION

Space Surveillance and Tracking (SST) is becoming more critical due to the current and expected growth of the earth orbiting population. As of January 2021, the number of Resident Space Objects (RSOs) greater than 10 cm in size registered by the U.S. Space Surveillance Network climbs up to $21,901$, the 71 % of which are not related to either active or ceased operations [1]. Additional threats are envisaged due to the deployment of mega-constellations aimed at providing global internet coverage. Starlink and OneWeb are two examples, currently accounting for almost 1,600 satellites in Low Earth Orbit (LEO). Procedures to efficiently build and maintain RSO catalogs are deemed necessary to ensure the continuation of space operations in the near future, se e.g. [2, 3]. In this regard, Space Surveillance and Tracking (SST) systems retrieve observations from a wide variety of both ground and space-based sensors and build a labeled map of RSOs through the so-called *observation-correlation process*.

Based on RSO catalogs, detection of potential conflicts can be automated and managed by Space Traffic Management (STM) entities. Operators are then relieved from conflict detection, only being warned and asked for resolution if required. This framework is convenient to ensure the safe and orderly growth of space operations in the era of space tourism and space-based global internet coverage. SST systems determine whether an incoming (uncorrelated) observation: 1) belongs to an already cataloged object, 2) can be associated to a previous uncorrelated observation to create a new object or 3) shall remain uncorrelated. This process, known as *observation-correlation*, requires the implementation of orbit determination, orbit propagation and data association methods. Coherence between these methods is critical for the provision of SST services in an operational environment, which imposes certain limits on the computational burden. Besides, operational spacecraft are found to perform maneuvers that may stem from mission requirements or collision avoidance. Maneuver detection and estimation further complicates the *observation-correlation* process, introducing additional complexity to the problem, as the space accessible to a given object is *a priori* infinite. Bounds for feasible maneuver efforts and gating for maneuver estimation scenarios must be properly defined, together with a reasonable approach for maneuver estimation.

The aim of the present work is thus to identify the current needs in maneuver detection methods applied to optical survey scenarios and propose a solution that can be used to accurately represent the character of maneuvers of RSOs in a statistical manner. The proposed approach relies on 1) the definition of an *admissible region* based on a novel control distance metric, and 2) the use of a statistical filtering framework in which hypotheses are generated from the admissible space conditioned on one or multiple measurements and previously characterized maneuvers. Accordingly, Section 2 provides an extensive re-

view on maneuver detection and estimation methods applied to the particular problem of space object tracking. The definition of an *admissible region* based on a control distance metric is covered in Section 3, aimed at characterizing the space accessible to a maneuvering RSO in terms of expected control effort. A novel and efficient control distance metric is presented in Section 4, which is then compared to state-of-the-art approaches. The proposed statistical framework is discussed in Section 5, where different approaches for post-maneuver state recovery based on Markov Chain Monte Carlo (MCMC) methods are presented. Section 5 also deals with the definition of heuristics based on already characterized maneuvers, together with a procedure to elaborate, promote and discard maneuver hypotheses. Results are obtained in a simulated scenario representative of a typical SST optical survey, which is described in Section 6. These results focus on the ability of the proposed method to solve the measurement association problem, properly detect maneuvers and accurately recover the post-maneuver state of the target RSO. Finally, conclusions and future extensions to this work are provided in Section 7, where the adequacy of the method to fulfill the current needs in maneuver detection and estimation is also analyzed.

2. MANEUVER DETECTION AND ESTIMATION METHODS APPLIED TO SST

The Earth orbital space is typically characterized by quiescent objects, whose position is highly dependant on environmental factors such as Earth's oblateness, the presence of third bodies, solar radiation pressure and atmospheric density. Models of varying complexity exist for determining the effects of these force fields on RSOs, which can be extremely useful for tracking purposes in cluttered regions. These models serve as the effective link between different observations of the same object, yet deemed to fail during maneuvering intervals. It is thus desirable to automatically infer when an object has maneuvered to properly keep track of the earth orbiting population.

Maneuver detection and estimation methods, being an extension of tracking algorithms, are significantly affected by the information available and the quality and timeliness of such information. In this regard, space surveillance typically employs two types of ground-based sensors: radars and optical telescopes. While the former are capable of determining the entire state of an RSO, including its radar cross section in some cases, the latter only provide line-of-sight data, i.e. angular data. Radars can operate under all lighting conditions, whereas telescopes have limitations regarding the amount of environmental light and the relative brightness of visible space objects. Moreover, keeping track of fast objects such as low altitude satellites is further complicated by the necessity of rapidly adapting the pointing direction. Optical telescopes are thus normally relegated to the observation of RSO that fall beyond the scope of current radar technology, i.e. Medium Earth Orbit (MEO) altitudes or above. MEO and GEO object observations feature a revisit time for a still telescope of (at most) once per night (twice in survey operations), which may even be of the order of days depending on the space surveillance strategy. The partial character of such observations coupled with the relatively long re-observation time, renders the problem of maneuver detection and, especially, estimation challenging. It is the objective of the current section to discuss on the main approaches to maneuver detection and estimation in the context of space surveillance, with a special interest on optical observations. There are mainly four types of methods for maneuvering target tracking of space objects:

- *Perturbed Dynamics:* rely on the use of State Transition Matrices for approximating the effects of maneuvers in the orbital motion. Maneuvers are then characterized via parameter estimation methods such as Non-Linear Batch Least Squares, see for instance the work by A. Pastor et al. [4].
- *Multiple Models:* additional models are considered for the target motion, typically varying the level of process noise or augmenting the number of state variables to be estimated. The active model is then marginalized based on measurement association metrics. Examples can be found in the work of B. Jia et al. [5] and J. Katzovitz [6].
- *Heuristics:* a statistical characterization of previous maneuvers can be performed using kernel density estimators [7] or machine learning algorithms [8]. New maneuvers are then approximated by means of the so-called *patterns of life*, or heuristics.
- *Optimal Control:* fitting a new observation can be posed as an optimal control problem. It is then possible to derive mismodeled dynamics or characterize the optimal maneuver subject to a defined cost function. In this regard, one can find the work of M. Holzinger et al. [9], D. Lubey [10] or the more recent proposal by R. Serra et al. [11] focused on track association.

The perturbed dynamics approach seems to be the most usual procedure to account for maneuvering targets as it relies on the main methods used for orbit determination. The assumption of a fixed number of maneuvers does not seem to hinder the applicability of the method since two maneuvers are sufficient to switch between two arbitrary orbits. Nevertheless, the accuracy may be affected by the approximations used to infer the effects of maneuvers in the object dynamics, especially for relatively long propagation times and high maneuver magnitudes. Also note that post-maneuver state estimation is partially or entirely conditioned on the control effort, and such control effort only regards the observed states. In general, a maneuver needs not necessarily correspond to an optimal transfer and if so, such optimal transfer is conditioned on the full state of the final orbit.

By carefully analyzing the diverse multiple model formulations, one may realize they are intended to work

in a rather benign environment. Their primary use may be limited to operator surveillance, close formations and, in general, low re-observation time scenarios. Nonetheless, the application of Interacting Multiple Model (IMM) methods is not deemed to fail if a sufficiently close definition of the maneuvering modes is proposed such as, for instance, orbit raising modes for electric propelled spacecraft and East-West / North-South Station Keeping modes for GEO operational satellites.

Heuristics, and in particular the use of historical data, has shown to bring in many benefits in a wide range of applications. Estimation in data sparse systems, as is the case for tracking of space objects with long re-observation times, can be eased by incorporating prior information regarding the expected behavior of the target. It is obvious that in the absence of previous data, these methodologies are hardly applicable, in which case they might be augmented with some of the alternatives discussed in this work. Moreover, dissimilar maneuvers performed due to other concerns, e.g. collision avoidance or transfer to graveyard orbits, may present difficulties in the ability to estimate the post-maneuver state.

Maneuver detection and characterization via optimal control is a promising solution in the absence of prior information about the target, or when heuristics-based approaches have shown to fail. The latter may well be the case for outlier maneuvers such as collision avoidance, failure conditions or re-positioning. Nonetheless, the assumption of continuous thrust may yield inaccurate post-maneuver state estimates for maneuvers requiring a high control effort or RSOs equipped with chemical propulsion systems.The assumption of fuel-optimal maneuvers represents the willingness of operators to extend the operational life of their satellites. Note, however, this assumption is conditioned on a final orbit. Thus, determining the fuel optimal transfer to a final optical track may lead to significant errors in the post-maneuver state estimate.

In order to fulfill the gaps in the current methodology, our proposal is strongly focused on the statistical characterization of the target state. The latter is thus relieved from the usual Gaussian and uni-modal assumptions, which allows the treatment of multiple maneuver hypotheses in the form of multiple modes featuring an arbitrarily complex distribution. These hypotheses may be based on optimal control or *patterns of life*, making an efficient use of the information available. Decision making, i.e. hypothesis testing, is ultimately based on both measurement association and control distance metrics.

3. ADMISSIBLE REGION BASED ON CONTROL DISTANCE

Hereafter, we propose an alternative method for the canonical Constrained Admissible Region (CAR) approach [12], tailored to the needs of maneuvering space objects. The CAR method is applicable to short arc tracklets or very short arcs, typically obtained in automated Charge-Coupled Device (CCD) space surveys. The sky is swept in search of objects, which appear as bright spots on a telescope lens (to which the CCD is attached) but since a significant area of the sky is to be covered, the duration of each individual observation (or fixed telescope pointing) is limited to a few minutes. These optical observations yield line-of-sight measurements (α-δ pairs) at different epochs, for which preliminary orbit determination methods exist [13]. Nevertheless, due to the short duration of the observations, the perceived objects often travel a very short arc, thereby hindering the applicability of usual preliminary orbit determination methods. A. Milani et al. [12] developed a methodology to deal with these type of observations. They realized that due to the short arc traveled by the object, the additional information obtained by these closely separated observations was very limited. It is then possible to reduce such observations, commonly referred to as tracklets, to a single line-of-sight and its time derivative (*Attributable*, given by α, δ, $\dot{\alpha}$, $\dot{\delta}$) at the mean epoch of the observations without a significant loss of information. It is clear that a single observation is insufficient to determine the state of a space object as there is no information regarding its range and range-rate (ρ, $\dot{\rho}$). However, certain constraints can be applied to the latter depending on the expectations about the observed object: it is possible to define Admissible Regions for space objects of different orbital regimes. Consider for instance the difference in the expected values of range and range-rate between a solar-orbiting asteroid and an Earth-orbiting artificial satellite.

Originally, the concept of Admissible Regions was applied to the observation of deep space objects such as comets or asteroids [14]. The increase in RSOs has raised the interest in Space Surveillance and Tracking (SST) and triggered the appearance of Space Situational Awareness (SSA), which can be defined as: “the knowledge required to detect, predict, avoid, operate through, recover from, and/or attribute cause to the loss or degradation of space activities” [15]. These, together with the availability of an extense network of optical telescopes that can be devoted to space surveillance, yield a high number of very short arc (VSA) observations that are to be assigned to space objects: either already catalogued or newly detected. A revisit of the Admissible Region was then proposed for this application, the Constrained Admissible Region [16]. The latter is based on defining a feasible set of ranges and range-rates given expected values (boundaries) for the eccentricity and semi-major axis, as opposed to the orbital energy and range metrics approach used in the original methodology to identify asteroids. There are numerous works on the application of the CAR for Initial Orbit Determination (IOD) and tracking. K. DeMars et al. [17] propose a statistical characterization of the CAR based on Gaussian Mixture Models applied to IOD of near geostationary space objects. T. Kelecy and J. Moriba [18], on the other hand, follow a Multiple Hypothesis method (CAR-MHF), in this case to track the orbital debris generated after a LEO object breakup. Similarly, J. Stauch et al. [19] propose a similar approach to the breakup of a geostationary object, adapting the CAR-MHF to deal with longer re-observation

times by means of a smoothing recursion. L. Pirovano et al. [20] recently published an interesting work covering the different IOD approaches derived from the Admissibile Region and *Attributable* concepts, suggesting a Differential Algebra IOD method that ultimately shows the loss of information derived from the use of *Attributables* as opposed to complete tracklets. They agree that for certain types of observations, a linear regression of the tracklets not only yields the same level of information but can be used to decrease the uncertainty [21]. In particular, this applies to short duration observations of GEO objects whose apparent motion is close to null. However, when the arc traveled by the object is sufficiently large, non-linearities of the object motion render this approach unusable and a higher-order regression or direct use of the raw data is recommended.

The method proposed here is primarily aimed at solving the track association problem considering maneuvers for optical survey scenarios and, as such, relies on *Attributables* as observation data. Typical bounds for the CAR, given in terms of semi-major axis and eccentricity, are found to cover a very broad region of the ρ-$\dot{\rho}$ space, thus not being well-suited for maneuver detection. Through the use of an efficient control distance metric, it is possible define proper bounds on the Admissible Region. These bounds may be based on a maximum expected control effort in absolute or relative terms. To this end, the nearest post-maneuver state in terms of control distance $\mathbf{x}_{est}$ needs to be determined. Based on this estimate and its associated control distance, ΔV_{est}, bounds for the space accessible to the object in terms of control effort are determined as:

$$\Delta V_{th} = \min\left(\Delta V_{max}, \max(\Delta V_{min}, k_{rel}\Delta V_{est})\right) \quad (1)$$

where ΔV_{max}, ΔV_{min} represent maximum and minimum absolute thresholds and k_{rel} is a factor used to define a maximum relative threshold. Following this approach, the entire region satisfying $\Delta V(\rho, \dot{\rho}) \leq \Delta V_{th}$ is assumed accessible to the object.

In Section 4, the definition of a novel and efficient control distance metric is provided, especially suited to the CAR approach based on control effort described in previous paragraphs. Section 5 presents an example of how the proposed CAR alternative can be embedded into an operational framework to solve the maneuvering target tracking problem for space objects in optical survey scenarios.

4. CONTROL DISTANCE METRIC DEFINITION

One of the most relevant issues related to maneuver detection methods is whether to perform maneuver characterization or not. In general, the probability of performing a maneuver of a given magnitude is highly correlated with its cost, e.g. in terms of fuel. The latter is especially true for operational satellites since their amount of on-board propellant is highly limited by design and re-fueling is usually not an option. Thereafter, properly characterizing the control cost can greatly increase the performances of maneuver detection methods.

In some applications, such as optical survey scenarios, the sparsity of data renders high-fidelity maneuver estimation methods rather inefficient: the time-of-flight between the pre- and post-maneuver observed states is so high that there is a significant number of locally optimal maneuvers featuring similar control magnitudes. This, coupled with the fact that high-fidelity models involve a relevant computational cost, lead to the exploration of approximate or surrogate models for maneuver characterization. These models need not represent the actual physical process undergone by the object neither determine a maneuver sequence close to the optimal one, but provide a sufficiently close estimation of the control effort (e.g. proportional to the optimal real solution) required to acquire the post-maneuver orbit from the pre-maneuver one. Thereby, one can refer to the output of this surrogate model as a *control distance metric*, since it provides a metric for the relative distance between two orbits in terms of the required control effort to move from one to the other.

In the following, a novel control distance metric based on a double impulsive burn is presented in Section 4.1. Such metric relies on the linearization of Gauss Planetary Equations upon the application of a sudden velocity variation. An implementation of the state-of-the-art in control distance metric definition is presented in Section 4.2. A comparison between both approaches is presented in Section 4.3, emphasizing on the ability of both metrics to characterized the unobserved space in the presence of a single post-maneuver optical track.

4.1. Double-Burn Keplerian Transfer

A relevant aspect in determining the optimal impulsive maneuver to acquire a certain target orbit is associated with the relative geometry of the initial and final trajectories.

$$\begin{bmatrix}\Delta p\\ \Delta f\\ \Delta g\\ \Delta h\\ \Delta k\\ \Delta L\end{bmatrix} \approx \begin{bmatrix} 0 & \frac{2p}{w}\sqrt{\frac{p}{\mu}} & 0 \\ \sqrt{\frac{p}{\mu}}\sin(L) & \sqrt{\frac{p}{\mu}}[(w+1)\cos(L)+f]\frac{1}{w} & -(h\sin(L)-k\cos(L))\frac{g}{w} \\ -\sqrt{\frac{p}{\mu}}\cos(L) & \sqrt{\frac{p}{\mu}}[(w+1)\sin(L)+g]\frac{1}{w} & (h\sin(L)-k\cos(L))\frac{f}{w} \\ 0 & 0 & \sqrt{\frac{p}{\mu}}\frac{s^2\cos(L)}{2w} \\ 0 & 0 & \sqrt{\frac{p}{\mu}}\frac{s^2\sin(L)}{2w} \end{bmatrix} \begin{bmatrix}\Delta V_r\\ \Delta V_\theta\\ \Delta V_h\end{bmatrix} \quad (2)$$

By performing one single impulsive maneuver, it is only possible to transfer to a final orbit that intersects the prior one, and it will do so in the exact maneuver location. Thereafter, two impulsive maneuvers are a sufficient (and necessary) condition to transfer between two arbitrary orbits. Another relevant aspect of impulsive maneuver design is the high impact of the burn location on the required velocity increment ΔV. This is especially relevant when considering two impulses since there are infinitely many pairs of burns that are compliant with a given transfer, but only a reduced set features an affordable control effort. Since our objective is to provide a control metric that can be applied to arbitrary initial and final orbits, a two-impulsive burn approach will be adopted. Moreover, it is desirable to reduce the computational complexity to the minimum, and so the transfer will be assumed to occur between two keplerian orbits, i.e. maneuvers are to be determined assuming unperturbed orbits.

The Gauss Planetary equations present a convenient formulation to develop a surrogate method for characterizing impulsive maneuvers. Expressed in Modified Equinoctial Elements [22], they take the form given by Eqs. 18-23 in Appendix A. This system of first order differential equations can be used to model the dynamics of an object subject to the gravitational field of a primary, with central parameter $\mu = GM$. In the case of a keplerian (unperturbed) orbit, the radial, azimuthal and normal perturbing accelerations a_r, a_θ, a_h are assumed to be null so that every orbital element is kept constant except for the anomaly, i.e. the angle that determines the location in the orbit as a function of time, which in this case is given by the true longitude L. More importantly, one can take advantage of the definition of the Gauss Planetary Equations to infer the effect of a sudden velocity variation in the orbital elements. To this end, the right hand side of Eqs. 18-23 can be integrated in an infinitesimal time, during which a Dirac's delta acceleration is applied $(a_r, a_\theta, a_h) \sim \delta(t - t_M)$. Note the latter involves solving a multi-dimensional integral with the initial and final orbits as boundary conditions.

An approximation to this integral is obtained under the assumption that the main contribution for the change in orbital elements is caused by the sudden velocity increment, so that the orbital elements are assumed to remain constant during the (infinitesimal) maneuvering interval. Thereafter, the instantaneous effect of an impulsive burn ΔV in the prior orbit is approximated by the linear system in Eq. 2. The error committed in estimating the effect of a given burn by means of the previous approximation can be consulted in Appendix B, where the maximum relative error in characterizing the maneuver given the post-maneuver state is bounded by a 10 % for orbits featuring virtually any inclination and eccentricity value under a nominal impulsive burn of $\Delta V_r \equiv \Delta V_\theta \equiv \Delta V_h = 10\ m/s$.

Based on these results, it follows the derivation of a method to fully determine the control effort required to transfer between two different orbits (given by the vectors of Modified Equinoctial Elements œ_0 and œ_2) in a specific amount of time. The aim is to obtain the minimum ΔV compliant with a given variation in orbital elements $\Delta\text{œ} = \Delta\,[\,p\ f\ g\ h\ k\,]$ such that:

$$\begin{aligned}\Delta\text{œ} &\equiv \Delta\text{œ}_1 + \Delta\text{œ}_2 \\ &= A(\text{œ}_0, L_1)\Delta V_1 + A(\text{œ}_1, L_2)\Delta V_2\end{aligned} \tag{3}$$

Where the term $A(\text{œ}_1, L_2)$ can be linearly approximated as:

$$\begin{aligned}&A(\text{œ}_1, L_2) \approx \\ &\quad A(\text{œ}_0, L_2) + \left.\frac{\partial A(\text{œ}_0, L_2)}{\partial \text{œ}}\right|_{\text{œ}_0} A(\text{œ}_0, L_1)\Delta V_1\end{aligned} \tag{4}$$

Thereafter, it is possible to solve for the couple of burns:

$$\begin{aligned}\Delta V &\equiv [\Delta V_1 \quad \Delta V_2]^T \\ &= \left((A_1 + A_2)^T(A_1 + A_2)\right)^{-1}(A_1 + A_2)^T\Delta\text{œ}^*\end{aligned} \tag{5}$$

where $A_1 = \begin{bmatrix} A(\text{œ}_0, L_1) \\ 0 \end{bmatrix}$ and $A_2 = \begin{bmatrix} 0 \\ A(\text{œ}_1, L_2) \end{bmatrix}$. Note that the linear term in Eq. 4 is dropped as otherwise the problem would have a second order term on $\Delta V_1, \Delta V_2$. In fact, one can apply predictor-corrector scheme on A_2 as follows:

$$A_2^{k+1} = A_2^k + \left.\frac{\partial A_2^k}{\partial \text{œ}}\right|_{\text{œ}_0} A_1\Delta V_1^k \tag{6}$$

In general, we are concerned about solving a modified problem, since the goal is to determine the optimal maneuver, instead of simply a compliant one. The solution proposed in Eq. 5 may lead to an over estimation of ΔV_1, counteracted through ΔV_2 so that the overall residuals $((A_1 + A_2)\Delta V - \Delta\text{œ}^*)^T((A_1 + A_2)\Delta V - \Delta\text{œ}^*)$ are minimized. An alternative solution can be devised by defining a cost function as:

$$J = \Delta V^T\Delta V + c_1(\Delta\text{œ}^* - \Delta\text{œ})^T(\Delta\text{œ}^* - \Delta\text{œ}) \tag{7}$$

being c_1 some scaling parameter, $\Delta\text{œ}^*$ the desired change in orbital elements, and $\Delta\text{œ}$ the change in orbital elements implied by the burn couple ΔV as given by Eq. 3. Then, one can simply equate the partial derivative of this function with respect to ΔV to zero, thereby leading to:

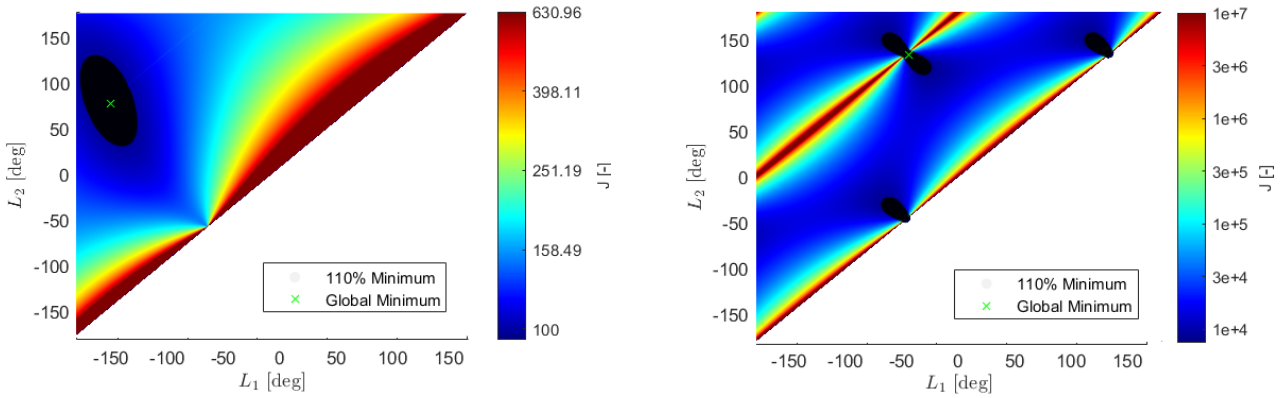

Figure 1: Loss function J vs $[\, L_1,\ L_2\,]$ for a GEO East-West (left) and North-South (right) station keeping maneuvers. The black shaded area comprises the region with a loss function value lower or equal than 110% of the global minimum, the latter being indicated by the green cross.

$$\begin{aligned}\frac{\partial J}{\partial \Delta V} =& 2\left(I + c_1(A_1+A_2)^T(A_1+A_2)\right)\Delta V \\ &- 2c_1(A_1+A_2)^T\Delta\text{œ}^* \equiv 0\end{aligned} \tag{8}$$

Thus resulting in the following expression for determining the fuel optimal pair of impulsive burns:

$$\begin{aligned}\Delta V = &\left(2\left(I + c_1(A_1+A_2)^T(A_1+A_2)\right)\right)^{-1} \\ &\cdot 2c_1(A_1+A_2)^T\Delta\text{œ}^*\end{aligned} \tag{9}$$

Note that Eq. 9 can be regarded as a generalized solution to the problem since if c_1 is set to zero, the expression in Eq. 5 is recovered. In either case, the predictor-corrector scheme defined in Eq. 6 can be applied on A_2 to improve the validity of the approximation in the intermediate transfer orbit, for which convergence is typically achieved after a reduced number of iterations (5-10).

The solution given by Eq. 9 is completely defined for a relative change in orbital elements $\Delta\,[\,p\ f\ g\ h\ k\,]$ and the pair of true longitudes $[\,L_1,\ L_2\,]$ at which the burns are performed. It is then possible to determine the optimal couple of true longitudes that lead to the minimum value of the loss function J introduced in Eq. 7. Fig. 1 depicts the behavior of J as a function of the true longitudes at which the impulses are applied. Therein, the global minimum is indicated with a green cross, whereas the region with a value not greater than 110% of such minimum is highlighted with shadowed circles. Despite only one local minimum is found for the East-West Station Keeping (EWSK) maneuver, the North-South Station Keeping (NSSK) one presents three well separated valleys. This behavior of the loss function is critical for the selection of the solver used to determine the optimal $[\,L_1,\ L_2\,]$ couple. In the case at hand, a simple Gauss-Newton method with multiple initial guesses seems to be a good compromise between a proper exploration of the solution space and efficiency in terms of computational cost.

4.2. Optimal Control Approach

The state of the art in maneuver detection and estimation methods propose an optimal control based approach to detect the existence and approximate the character of maneuvers of RSOs [9, 23, 24, 11]. In this regard, a continuous thrust model is usually adopted, establishing upper and lower bounds for the maximum control acceleration. The outcome of the Optimal Control Problem (OCP) can be synthesized to the integral of the control acceleration over the prescribed time of flight, which formally defines a proper control distance metric. The non-linear optimization problem may be expressed as:

$$\begin{aligned}&\text{Minimize} \quad J = \tfrac{1}{2}||x_f - x(t_f)||^2 + \tfrac{1}{2}\int_{t_0}^{t_f}\mathbf{x}_c^T\mathbf{x}_c\,dt \\ &\text{subject to:} \quad x(t_0) = x_0 \quad \tfrac{dx}{dt} = f(x,t,\mathbf{x}_c)\end{aligned} \tag{10}$$

Where $\mathbf{x}_c$ is the control acceleration vector, and x_f, x_0 are the final and initial boundary conditions, respectively. In this work, the control metric considered is directly related to the second term of the loss function in Eq. 10, usually referred to as *lagrangian* in optimal control theory. As in the previous case (see Section 4.1), the control effort is regarded as an increase in orbital velocity so that the distance metric ΔV is given in velocity units and defined by:

$$\Delta V = \sqrt{2P} \qquad P = \frac{1}{2}\int_{t_0}^{t_f}\mathbf{x}_c^T\mathbf{x}_c\,dt \tag{11}$$

The OCP is solved using a direct collocation method, in which the dynamical model is given by the unperturbed

Gauss Planetary Equations expressed in Mean Equinoctial Elements. CasADi [25] framework is used to pose the Non-Linear Programming (NLP) problem, and the selected NLP solver is WORHP [26], mainly due to its robustness and computational efficiently when compared to the well-established open source alternative IPOPT [27].

4.3. Control Distance Metrics Comparison

A comparison is drawn between the aforementioned control distance metric based on continuous thrust and the impulsive burn approach developed in Section 4.1. The intended application scenario is composed of known maneuvering objects observed from ground-based telescopes. Under these settings, only the line-of-sight $\mathbf{r}$ (α-δ pair) and its first time derivative $\dot{\mathbf{r}}$ are observed, so that information regarding the range ρ and range-rate $\dot{\rho}$ needs to be estimated in order to determine the full state of the RSO. These are typically inferred from already cataloged objects whose trajectory is well characterized, at least for pure ballistic (or uncontrolled) motion. In the presence of (unknown) maneuvers, the post-maneuver state of an object cannot be accurately estimated but rather hypothesized, usually in terms of range and range-rate values. These ρ-$\dot{\rho}$ hypotheses are thus built upon the observation, rendering association metrics such as Mahalanobis distance, measurement likelihood or observation residuals useless. It is then convenient to use alternative metrics, e.g. based on a control effort, to evaluate the hypothesized states.

In the following, the ability of the metrics presented in Sections 4.1 and 4.2 to properly describe and characterize the state space in terms of the unobserved variables ρ-$\dot{\rho}$ is to be assessed. Results are obtained for two different cases: a) an East-West Station Keeping (EWSK) maneuver and b) a North-South Station Keeping (NSSK) maneuver, both performed by a Geosynchronous (GEO) RSO. The solution space in terms of the control distance metrics is depicted in Fig. 2 for the EWSK maneuver and Fig. 3 for the NSSK one. Therein, the true post-maneuver state is given by the $(0, 0)$ coordinates and the control distance metric is referred to the ballistic estimate at the post-maneuver observation epoch. The assumed time of flight in both cases is one sidereal day.

From the figures, contour lines for the distance metric based on optimal control are seen to be tilted ellipses with a positive $\Delta\rho$-$\Delta\dot{\rho}$ correlation. This is the expected behavior for the case of limited control authority, as the momentum gain required to reach high $|\Delta\rho|$ is necessarily given by $\Delta\dot{\rho}$ values of the same sign. This directional behavior is not so evident in the impulsive approach, where only a mild effect can be observed for the EWSK case near the diagonal. Another relevant difference between both approaches is the relative value of the control metric itself, being almost one order of magnitude lower in the impulsive case. Nonetheless, this is simply a relative scaling that mimics the effect of gravity losses and does not have further implications in the usability of the con-

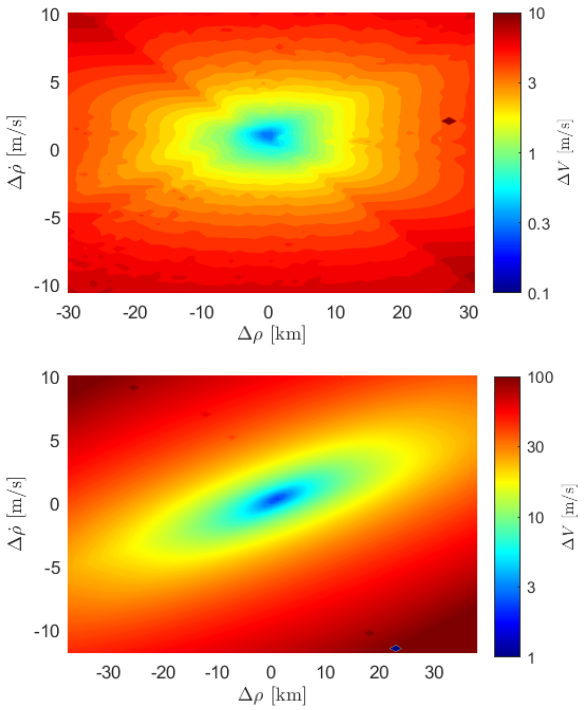

Figure 2: Impulsive (top) and continuous thrust (bottom) control distance metric as a function of range and range-rate differences for an EWSK maneuver.

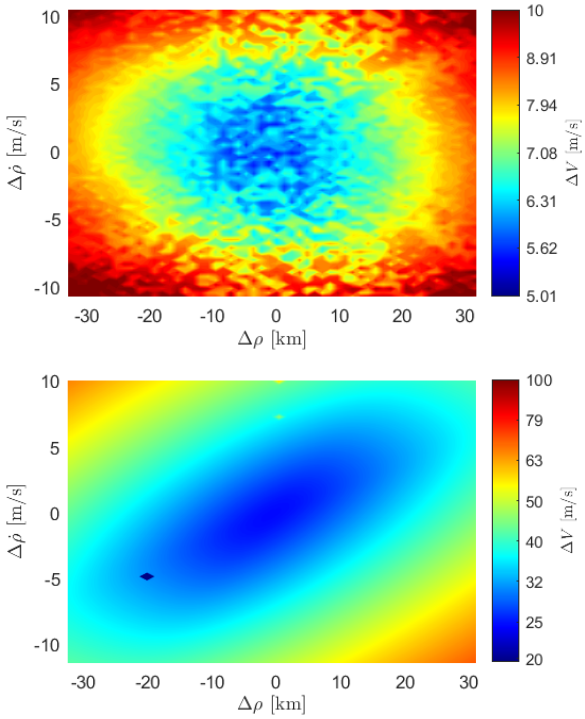

Figure 3: Impulsive (top) and continuous thrust (bottom) control distance metric as a function of range and range-rate differences for a NSSK maneuver.

trol distance metric, i.e. similar admissible spaces are obtained for 10 and 100 m/s thresholds on the impulsive and continuous thrust approaches, respectively. With regard to the impulsive based control distance metric, a non-smooth behavior can be observed for the NSSK maneuver (see Fig. 3), despite the overall trend being captured. This is thought to be caused by the presence of multiple local minima (as already inferred from Fig. 1) and the inability of the optimization scheme to properly determine the global minimum.

Overall, both metrics give a similar insight into the problem provided a proper scaling is applied to leverage the raw distance metric magnitude. The optimal control approach presents a smoother behavior as convergence to the global minimum seems to be ensured. This comes at the cost of a greater computational burden, since a high-dimensional non-linear optimization problem needs to be solved. Moreover, the size of the NLP problem increases with the time of flight as more discretization (or collocation) points are required to properly capture the dynamics. The proposed control distance metric based on impulsive burns is free from these limitations since the time of flight only affects the admissible true longitude region, i.e. those values that are feasible within the specified time span. A reduction in computational time of up to one order of magnitude is also experienced, from an expected execution time of 700ms for the OCP to 90ms in an Intel Core i7-8750H laptop CPU. Thereafter, this novel approach has proved to deliver an efficient control distance metric, generalized to consider impulsive maneuvers and readily applicable to optical observation scenarios.

5. SEQUENTIAL MONTE CARLO FOR MANEUVERING SPACE OBJECTS

Sequential Monte Carlo (SMC) methods have been successfully applied to maneuvering target tracking problems in the presence of high measurement uncertainty (see for instance [28, 29]), and so they are expected to deliver reasonable performances in data sparse scenarios as is the case of maneuvering space objects. SMC relies on the use of sampled populations for approximating the state distribution of a target in order to solve the state space filtering problem. Treatment of individual observations or measurements is done in a sequential manner, so that the sampled distribution that approximates the target state is updated at each incoming observation. This population may take any realization, rendering SMC filters suitable for applications in which the state distribution is non-gaussian and/or multi modal.

SMC methods provide natural support for multiple hypotheses, which may appear in the form of clearly separated modes in the sampled space. These hypotheses can be elaborated based on measurement association considering maneuvers. Hypothesis pruning and promotion is then performed according to their ability to associate with more recent observations so that at some point, only the true hypothesis survives.

In the following, methods for inferring the post-maneuver state distribution by means of a control distance metric are developed in Section 5.1. Section 5.2 presents an overview of how hypotheses are generated and promoted based on the measurement sequence. Section 5.3 deals with maneuver characterization methods and the definition of heuristics that can be used to approximate future maneuvers. Finally, Section 5.4 discusses on the proposed SMC framework for solving the maneuvering target tracking problem applied to optical observations.

5.1. Post-maneuver State Estimation via MCMC

For some applications, there is not a clear definition of the dynamical model governing the state evolution of the target. In these cases, an alternative procedure is given by Markov Chain Monte Carlo (MCMC) methods, which focus on the exploration of the *posterior* distribution disregarding the underlying physical processes.

In the case of maneuvering space objects, one may assume the dynamics to be unknown during maneuvering intervals, and focus on determining a sufficiently accurate state estimation after the maneuver. In doing so, the definition of an Admissible (control) Region, as given in Section 3, can be of aid. Based on a control distance metric ΔV, bounds for the admissible set of range ρ and range-rate $\dot{\rho}$ values are defined, e.g. according to Eq. 1. These bounds can then be used to build a hypothesized state distribution conditioned on the post-maneuver measurement $p(\mathbf{x}|\mathbf{y})$ or measurement sequence $p(\mathbf{x}|\mathbf{Y})$. These two cases are very different in terms of the information available, and so the methods used to sample from the post-maneuver state distribution.

5.1.1. Single Track after the Maneuver

When only a single track is available after the maneuver, the expected correlation between the post-maneuver state and the control distance metric is high. In the proposed approach, the state is assumed to be divided into two clearly distinguishable sets, the observed $\mathbf{o} = \left[\alpha\ \delta\ \dot{\alpha}\ \dot{\delta}\right]$ and the unobserved $\mathbf{u} = [\rho\ \dot{\rho}]$ variables. Since there is no information regarding the dynamical process undergone by the target, the observed set is assumed to follow the distribution given by the measurement uncertainty, i.e. $\mathbf{o} \sim \mathcal{N}(\mathbf{y}, \mathbf{Q})$, where $\mathbf{y}$ is the processed measurement data and $\mathbf{Q}$ the assumed measurement covariance.

A *proposal* distribution is defined for the unobserved set $\mathbf{u}$ based on the admissibility region, modeled as a Gaussian. This assumption is somehow compliant with the control distance metric distribution shown in Figs. 2 and 3, where there is one region of single or multiple local minima featuring elliptical outer contour lines. In order to build this Gaussian, five points need to be determined. The first, $\mathbf{u}_{est} = [\rho_{est}\ \dot{\rho}_{est}]$, is used as reference for determining the outer boundaries of the distribution, and is defined as:

$$\mathbf{u}_{est}: \quad \underset{\mathbf{u}}{\text{argmin}} \Delta V(\mathbf{u}, \mathbf{y}) \tag{12}$$

In essence, it is the state featuring the minimum control effort required to be compliant with a post-maneuver track. The remaining four points are given by:

$$\begin{aligned}
\mathbf{u}^+: &\quad \underset{\rho}{\text{argmin}} (\Delta V([\rho\ \dot{\rho}_{est}], \mathbf{y}) - \Delta V_{th})^2 \ \mid\ \rho > \rho_{est} \\
\mathbf{u}^-: &\quad \underset{\rho}{\text{argmin}} (\Delta V([\rho\ \dot{\rho}_{est}], \mathbf{y}) - \Delta V_{th})^2 \ \mid\ \rho < \rho_{est} \\
\mathbf{u}_+: &\quad \underset{\dot{\rho}}{\text{argmin}} (\Delta V([\rho_{est}\ \dot{\rho}], \mathbf{y}) - \Delta V_{th})^2 \ \mid\ \dot{\rho} > \dot{\rho}_{est} \\
\mathbf{u}_-: &\quad \underset{\dot{\rho}}{\text{argmin}} (\Delta V([\rho_{est}\ \dot{\rho}], \mathbf{y}) - \Delta V_{th})^2 \ \mid\ \dot{\rho} < \dot{\rho}_{est}
\end{aligned} \tag{13}$$

where ΔV_{th} is the maximum allowable control effort as defined in Eq. 1. The *proposal* $\pi(\mathbf{u})$ is then characterized by the four points in Eq. 13, using their mean $\langle \mathbf{u} \rangle = E\left(\mathbf{u}^+,\ \mathbf{u}^-,\ \mathbf{u}_+,\ \mathbf{u}_-\right)$ and variance $P = Var\left(\mathbf{u}^+,\ \mathbf{u}^-,\ \mathbf{u}_+,\ \mathbf{u}_-\right)$ as the k^{th} σ-contour so that $\pi(\mathbf{u}) \sim \mathcal{N}(\langle \mathbf{u} \rangle, kP)$.

Markov Chain Monte Carlo methods, and in particular Metropolis-Hastings ($\mathcal{MH}$) type algorithms [30], rely on the use of a *proposal* to determine the *target* or *posterior* distribution. Samples are randomly (or quasi-randomly) drawn from the proposal and accepted or rejected based on certain criteria. Note that for this approach to follow, the support of the *posterior* distribution must be contained within that of the *proposal*, i.e. the set of points with non-zero probability w.r.t. the *posterior* must also have non-zero probability w.r.t. the *proposal*. Exploration of the *posterior* is essentially based on a metric, usually the likelihood: samples featuring higher likelihood values are favoured over those with lower values. Thereafter, we propose to define the *target* distribution $p(\mathbf{x}|\mathbf{y})$ inversely proportional to the exponential of the control distance metric, i.e.:

$$p(\mathbf{x}|\mathbf{y}) \propto \exp(-\Delta V(\mathbf{x})) \tag{14}$$

In the present work the DiffeRential Evolution Adaptive Metropolis (DREAM) algorithm by J. Vrugt et al. [31] is selected, mainly due to its increased performance when compared to naive random-walk $\mathcal{MH}$ algorithms. DREAM uses a Metropolis selection rule to accept or reject samples drawn form a *proposal* distribution. These samples generate a chain or sequence of values that converges to the *target* as this chain is simulated, i.e. more samples are drawn. In fact, DREAM is a multi-chain algorithm, meaning that multiple chains are simulated in parallel to improve convergence and efficiency. The last n values of the different sequences are then incorporated into the population representing the state of the RSO, characterizing the accessible space conditioned on the last observation. Note that multiple hypotheses might stem from this process in case the *posterior* distribution presents a multi-modal shape.

5.1.2. Multiple Tracks after the Maneuver

If more than one track is available after the maneuver, the aim is to determine the state distribution conditioned on the track sequence $p(\mathbf{x}|\mathbf{Y})$. In fact, this scenario can be regarded as a refinement over the post-maneuver state estimated using a single post-maneuver track. The *prior* distribution is then known and effectively corresponds to the Admissible Region based on the control distance metric. At this point, it is of interest to determine the subset of the Admissible Region that is compliant with the track sequence. To this end, another type of MCMC algorithm is used: the Hybrid (or Hamiltonian) Monte Carlo ($\mathcal{HMC}$), proposed by S. Duane et al. [32]. In fact, $\mathcal{HMC}$ is a special kind of $\mathcal{MH}$ algorithm with a concrete definition of the proposal distribution. Initialization is performed via a single starting point x_0, whose dynamics are assumed to be subject to the Hamiltonian:

$$\begin{aligned}
\frac{dx}{dt} &= r \qquad \frac{dr}{dt} = \frac{\partial log(p(x|y))}{\partial x} \\
x(0) &= x_0 \qquad r(0) \sim \mathcal{N}(0, I)
\end{aligned} \tag{15}$$

These *fictitious* Hamiltonian dynamics are then simulated by means of a time-reversible and volume-preserving propagator, usually the fixed-step leapfrog scheme. Dynamics are propagated for L steps, resulting in a total fictitious propagation time $t_f = \varepsilon L$. Acceptance or rejection of the propagated particle x^{t_f} is based on a Metropolis Hastings update, i.e. if the ratio $\alpha = \frac{p(x^{t_f}|y)}{p(x^{t_0}|y)}$ is greater than some number $u \sim \mathcal{U}(0,1)$, then the sample x^{t_f} is accepted and will replace x_0 in the following iteration. Note that this sampling scheme is highly sensitive to the number of integration points and step size. Too small ε would lead to an inefficient sampling as each new proposal would be very similar to the previous one. High ε values lead to a greater exploration of the distribution while producing less likely proposals. Tuning L is further complicated by its local dependency on the dynamics. Hoffman et al. [33] propose a method to eliminate the need to define a number of steps. This method, coined the No U-Turn Sampler (NUTS), suggests building candidate points until those are found to make a U-Turn. Results therein presented show a significant increase in computational efficiency as one only needs to optimize a single parameter, the step size.

The proposed method suggests utilizing NUTS with a starting point selected from the population subset sampled according to the procedure described in Section 5.1.1. This point is then propagated to the subsequent measurement epochs and State Transition Matrices (STMs) for these transformations are obtained. The *posterior* distribution used in this case corresponds to the Bayesian definition $p(\mathbf{x}|\mathbf{Y}) \propto p(\mathbf{x}|\mathbf{y}_1)p(\mathbf{x}|\mathbf{y}_2)...p(\mathbf{x}|\mathbf{y}_N)$, being N the total number of post-maneuver tracks. The measurement likelihood for the entire track sequence is determined for each sample point, propagated using the aforementioned STMs. These

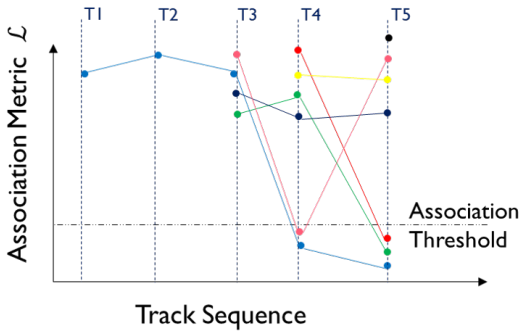

Figure 4: Hypothesis generation based on a typical post-maneuver track sequence. Different colors represent hypotheses based on different track sets.

STMs are updated whenever a sample significantly deviates from the reference point used to calculate them or after certain number of samples have been drawn. Again, a chain is simulated using NUTS and the last n values of this chain are incorporated into the population that approximates the state distribution of the target RSO at the last measurement epoch. This way, hypotheses based on the association of multiple post-maneuver tracks are generated, which can be used for instance to refine post-maneuver state estimates as new tracks become available.

5.2. Hypotheses Management

This section presents the rationale behind hypotheses generation, promotion and pruning. Decision making is based on the control metric derived in Section 4.1 and an association metric, the measurement likelihood $\mathcal{L}$. Similar to the threshold defined for the control distance metric, ΔV_{th}, another threshold is set for the measurement likelihood $\mathcal{L}_{th}$, which in this case is the result of a gating procedure based on the Mahalanobis distance [34] (see Section 5.3 in the thesis by J. Siminski [21]). This thresholding is used to detect maneuvers, i.e. if any particle $\mathbf{x}_i$ belonging to the population features an association metric $\mathcal{L}(\mathbf{x}_i) \geq \mathcal{L}_{th}$ then the track is assumed to belong to the RSO; otherwise the maneuver hypothesis is tested.

In the no-association scenario, the reference point specified in Eq. 12 is determined, and its corresponding control distance metric value ΔV_{est} is tested against the maximum allowable control effort given in Eq. 1. If lower, samples from the post-maneuver state distribution are drawn based on the procedure described in Section 5.1.1. Otherwise, if $\Delta V_{est} \geq \Delta V_{th}$, the track is not associated with the RSO and thus left uncorrelated.

As more post-maneuver tracks arrive, hypotheses are generated based on all the possible combinations. This is illustrated in Fig. 4, where the measurement likelihood of different hypothesis is shown as a function of the track sequence in chronological order. At T4, the ballistic (light blue) hypothesis is not compliant with the measurement, so maneuver hypotheses are built based on T4 alone (red) and the T3-T4 pair (green). Note that the maneuver might have been performed between T2 and T3 but the impact in the state could have been so low that the ballistic hypothesis is still capable of associating with T3. As T5 arrives, none of the previously generated hypotheses is able to associate so new hypotheses are generated based on T5 (black), the T4-T5 pair (yellow), the T3-T5 pair (pink) and the set T3-T4-T5 (dark blue).

This process is continued until a change is detected in the ballistic hypothesis, effectively conforming a maneuver detection. Selection of the ballistic hypothesis r_b is done according to the following criteria:

$$r_b(t_j): \quad \underset{r_k}{\text{argmax}} \sum_{m=0}^{n_w} \phi^{n_w-m} \max \mathcal{L}(\mathbf{x}_k(t_{j+m-n_w})) \tag{16}$$

where $\phi = 0.9$ is a forgetting factor used to give more weight to more recent tracks and n_w is a sliding window over which the selection of the ballistic hypothesis is smoothed.

With regard to pruning of the hypotheses, only those that are found to associate are maintained. Indeed, there is an exception to this rule as the ballistic hypothesis at each epoch is always kept in order to account for the no-maneuver scenario.

5.3. Maneuver Characterization and Heuristics

As mentioned in Section 5.2 above, a change in the ballistic hypothesis is considered a maneuver detection. At that point, both the pre- and post-maneuver orbits are assumed to be properly characterized; and so the maneuver. This maneuver is expected to occur right before the first track that associates with the new ballistic hypothesis, e.g. in Fig. 4 the ballistic hypothesis at T5 would correspond to the dark blue line so that the maneuver is isolated between T2 and T3. In order to characterize the maneuver, the population subsets corresponding to the pre- and post-maneuver hypotheses are compared. This comparison is translated into a distribution of relative variations in orbital elements, in particular the change in semi-major axis Δa, eccentricity Δe and inclination Δi. A reduced set of the classical orbital elements is chosen due to the target orbital regime, i.e. Geosynchronous orbits. Note that the relative change in mean longitude is disregarded as it is strongly affected by the relative timing of the maneuver with respect to the measurements and can be somehow estimated from the optical tracks themselves.

The outcome of comparing the pre- and post-maneuver populations is a multi-variate Gaussian distribution in $[\Delta a\ \Delta e\ \Delta i]$. As more maneuvers are characterized, a Gaussian Mixture Model with an increasing number of components is built. At some point, an expectation max-

imization algorithm can be used to merge similar maneuvers and reduce the size of the Gaussian Mixture.

In order to efficiently use information derived from historical maneuvers, a procedure similar to the one described in Section 5.1.1 is followed. The proposed approach still consists in using the DREAM algorithm to sample from the *posterior* distribution based on a *proposal*. In fact, the proposal is exactly the one described therein, so the only variation is the definition of the *posterior*. Each sample drawn during the MCMC simulation is compared against the ballistic reference state at the measurement epoch and the probability of belonging to the Gaussian Mixture Model used to characterized previous maneuvers is used as discriminant instead of the metric defined in Eq. 14. The latter procedure effectively provides a means to sample from the admissible control region conditioned on the information derived from previously characterized maneuvers.

5.4. Sequential Monte Carlo Framework

An overview of the proposed Sequential Monte Carlo method can be consulted in Algorithm 1. This scheme can be regarded as the upper level framework containing the procedures and methods described in Sections 5.1-5.3. The filter is initialized with a sampled population at the initial epoch. Such population is then propagated to the subsequent measurement epoch according to the non-linear dynamical model $f(\cdot)$ and an assumed process noise $w(\cdot)$. Measurement likelihood is then evaluated for the entire population to accept or reject measurement association. In the latter case, post-maneuver state hypotheses are elaborated based on the different MCMC methods presented in Section 5.1 as discussed in Section 5.2. Note that if a maneuver has been detected recently, the post-maneuver orbit is refined in step 3.2. The latter is usually required by the lack of information available at the first post-maneuver track and thus the inability to sample from the support of the post-maneuver state distribution at this point. A resampling step is then applied to replace those particles (and hypotheses) that do not associate with the measurement or fall beyond the admissibility region. Finally, a smoothing recursion is used to improve the measurement association and maneuver detection performance by incorporating future information to the problem. This recursion is only necessary near maneuver intervals, so when the active ballistic hypothesis changes (a maneuver detection is confirmed), the filter runs in pure sequential mode until a new maneuver hypothesis is generated.

6. RESULTS AND DISCUSSION

The proposed method is evaluated in a simulated optical survey scenario. The subject of study is a geosynchronous RSO performing East-West and North-South station keeping maneuvers to remain in its assigned slot.

Algorithm 1: Sequential Monte Carlo Approach

INITIALIZATION

Sample N particles $\mathbf{x}_{0,i}$ from $p(\mathbf{x}_0)$ with weights $\omega_{0,i} = \frac{1}{N}$

for $k > 1$ **do**

IMPORTANCE SAMPLING

1) Approximate $p(\mathbf{x}_k|\mathbf{Y}_k)$:

$$\omega^-_{k,i} = \omega_{k-1,i} \quad \mathbf{x}^-_{k,i} = f(\mathbf{x}_{k-1,i}, t_{k-1}) + w(t_{k-1})$$

2) Apply the measurement update to obtain $p(\mathbf{x}_k|\mathbf{Y}_{k-1})$:

$$\omega_{k,i} = \frac{\omega^-_{k,i} p(\mathbf{y}_k|\mathbf{x}_{k,i})}{\sum_{i=1}^{N} \omega^-_{k,i} p(\mathbf{y}_k|\mathbf{x}_{k,i})} \quad \mathbf{x}_{k,i} = \mathbf{x}^-_{k,i}$$

DETECT MANEUVER

3) Check association:

if $\max(\mathcal{L}(\mathbf{x}_{k,i})) < \mathcal{L}_{th}$ **then**

3.1) Simulate a Metropolis Hastings chain $\mathcal{MH}(\mathbf{y}_k)$ to obtain $\mathbf{x}^+_{k,i}$ as described in Section 5.1.1.

if *maneuver detected at* $\mathbf{y}_{k-j}$ **then**

3.1.1) Simulate a Hamiltonian Monte Carlo chain to obtain $\mathbf{x}^+_{k,i}$ as described in Section 5.1.2 considering all the possible measurement combinations $\binom{\mathbf{y}_{k-j:k}}{k}$, i.e. $\mathcal{HMC}\left[\binom{\mathbf{y}_{k-j:k}}{k}\right]$.

else

3.1.2) Simulate a Hamiltonian Monte Carlo chain $\mathcal{HMC}(\mathbf{y}_{k-1:k})$ to obtain $\mathbf{x}^+_{k,i}$ as described in Section 5.1.2.

else if *maneuver detected at* $\mathbf{y}_{k-j}$ **then**

3.2) Simulate a Hamiltonian Monte Carlo chain $\mathcal{HMC}(\mathbf{y}_{k-j:k})$ to obtain $\mathbf{x}^+_{k,i}$ as described in Section 5.1.2.

RESAMPLING

4) Compute the set of surviving particles Ω:

$$\Omega = \left\{ \mathbf{x}^+_{k,l} : \left[\Delta V(x^+_{k,l}) \leq \Delta V_{th}\right] \cup \left[\mathcal{L}(x^+_{k,l}) \geq \mathcal{L}_{th}\right] \right\}$$

if $\Omega \subsetneq x^+_{k,i}$ **then**

4.1) Compute the cumulative distribution of $p_s(\mathbf{x}_k|\mathbf{Y}_k)$:

$$P_s(\mathbf{x}_k|\mathbf{Y}_k) = \sum_{i \in \mathcal{I}(x)} \omega_{k,i} \quad \mathcal{I}(x) = \{i : x_i \leq x\}$$

4.2) Draw u_i from $\mathcal{U}(0,1)$ and update the particles $x^+_{k,i} \notin \Omega$ according to:

$$\omega_{k,i} = \tfrac{1}{N} \quad \mathbf{x}_{k,i} = \mathbf{x}_{k,j}$$

$$P(\mathbf{x}_{k,j-1}|\mathbf{Y}_k) \leq u_i \leq P(\mathbf{x}_{k,j}|\mathbf{Y}_k)$$

4.3) Retain a fraction of the population f_b belonging to the ballistic hypothesis $r_b(t_k)$.

SMOOTHING

5) Repeat steps 1-4 (obviating step 3.2) for all measurements up to the last detected maneuver, first backward and then forward in chronological order.

Observations are obtained for an optical sensor network consisting of two telescopes. The details of the proposed test scenario are summarized below:

- *Subject:* geosynchronous RSO equipped with chemical propulsion featuring a mean longitude slot $\ell = -4.8 \pm 0.2°$ and an inclination slot $i = 2 \pm 0.05°$. The object is simulated for a total duration of 400 days using a dynamical model including the following perturbations:
  - Non-spherical Earth of degree and order 70.
  - Third-body perturbations of Sun, Moon and Planets (including Pluto).
  - Cannonball model for the Solar Radiation Pressure (SRP) with a conical solar and lunar eclipse model, using fraction of illumination for penumbra regions.
  - Solid Earth and ocean tides.
  - General Relativity.
- *Optical Sensor Network:* two optical ground telescopes located at Zimmerwald (AIUB Zimmerwald's Observatory) and Tenerife (ESA Optical Ground Station). The optical survey presents the following characteristics:
  - Elevation mask of $20°$.
  - Solar phase angle between $0°$ and $9°$.
  - Angular distance to Earth shadow $\theta > 0°$.
  - Observation model for both right ascension α and declination δ featuring a zero-mean Gaussian noise with standard deviation $\sigma_{\alpha,\delta} = 1''$.
  - Mean revisit time of 1 day per site, as shown in Fig. 5.
  - Track length $T \sim \mathcal{U}(2.5, 15)$ min.
  - Tracks are reduced to the *Attributable* format by performing a linear regression with respect to the mean epoch.
  - Observation covariance is determined according to the time span and number of observations of a given track as suggested by J. Maruskin et al. [35], Eq. (8).
- *Proposed Method:* the proposed Sequential Monte Carlo Framework based on an admissible control region is configured as follows:
  - Thresholds for the admissible control region $\Delta V_{max} = 10$ m/s, $\Delta V_{min} = 1$ m/s, $k_{rel} = 3$.
  - The association gate is given by a 3-σ threshold considering a χ^2 distribution with 4 degrees of freedom.
  - Total size of the population is $N = 5000$ particles, and $N_{MC} = 500$ particles are sampled in every call to the DREAM and NUTS algorithms.

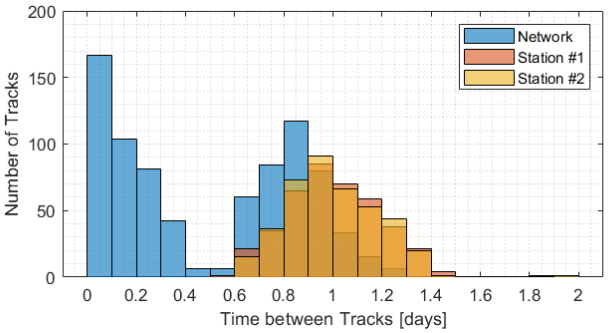

Figure 5: Histogram of re-observation time for the simulated optical sensor network.

  - The three cartesian components of position and velocity are estimated, together with the solar radiation pressure coefficient c_R.
  - Process noise w is included in the form of a random initial perturbation with standard deviation $[\sigma_x \ \sigma_v \ \sigma_{c_R}] = \left[10\,m \ 10^{-3}\,m/s \ 10^{-3}\right]/(t_k - t_{k-1})$, t expressed in days.
- *Alternative Method:* an alternative approach is considered for the sake of comparison. This approach uses a Non-Linear Batch Least Squares (BLS) that considers up to 6 subsequent measurements. Measurement association and maneuver detection is based on the same thresholds used in the proposed method, also considering the Admissible Region based in the developed control distance metric. Estimation is re-initialized after a maneuver is detected.
- *Dynamical Model:* the dynamical model used for state estimation both in the proposed and alternative methods have the following characteristics:
  - Non-spherical Earth of degree and order 5.
  - Third-body perturbations of Sun and Moon.
  - Cannonball model for the SRP with a conical solar and lunar eclipse model, using angular linear interpolation for penumbra regions.

A comparison between the proposed and alternative methods is then drawn based on 1) association and maneuver detection metrics and 2) post-maneuver state estimation accuracy. The former compares the ability of the methods to indicate a proper measurement association and correctly isolate the maneuver interval. Accuracy in terms of post-maneuver state estimation is given in the form of the Root Mean Squared Error (RMSE) as a function of the elapsed tracks (not time) since the maneuver. This RMSE is compared to the ground truth and given for the entire population (Pop) of the true hypothesis at epoch (not the ballistic one) and the maximum likelihood estimate (MLE) of each method.

	Association		*Maneuvers*	
	BLS	*SMC*	*BLS*	*SMC*
TP	793	795	20	20
TN	5	5	769	775
FP	0	0	9	3
FN	2	0	2	2

Table 1: Association and maneuver detection metrics for the proposed Sequential Monte Carlo (SMC) approach and the alternative Batch Least Squares (BLS) method.

6.1. Association and Maneuver Detection

Herebelow, the association and maneuver detection performances shown by the proposed Sequential Monte Carlo framework and a Non-Linear BLS approach are presented and discussed. Results are given as the number of true positives (TP), true negatives (TN), false positives (FP) and false negatives (FN) according to the decisions taken by the algorithms under evaluation. These results are summarized in Table 1, where the true negative associations are related to erratic observations caused by the selected measurement noise model. In terms of association, the proposed method is capable of correctly determining which tracks correspond to the target RSO. The BLS approach, on the contrary, presents two false negative associations, both in the vicinity of a maneuver. The latter is associated to an improper post-maneuver state estimation at the second track after the maneuver, so that the control distance required to reach the final orbit falls beyond the admissible bounds and association with this last track is discarded. The RSO performs a total of 22 maneuvers, 5 North-South and 17 East-West. As indicated in Tab. 1, both methods are capable of correctly isolating 20 maneuvers. In fact, the failure modes for the false negatives are similar in both cases, one maneuver is detected with a delay of one track and the other is combined with a previous maneuver occurring three tracks in advance. False positives are triggered by insufficiently accurate estimates of the post-maneuver states, so that additional maneuvers are required to recover a proper state definition. In either case, the most demanding scenario turned out to be NSSK maneuvers, for which post-maneuver state predictions present significant errors in semi-major axis and eccentricity. According to the association and maneuver detection performances obtained in the presented test scenario, the proposed method exhibited a superior performance when compared to an industry standard, i.e. the Non-Linear Batch Least Squares estimator. The measurement association problem has been properly solved and maneuver detection and isolation is better characterized, possibly due to the use of heuristics and a multiple hypothesis approach. Still there is room for improvement in the correct determination of maneuver intervals, which may be limited by observability conditions.

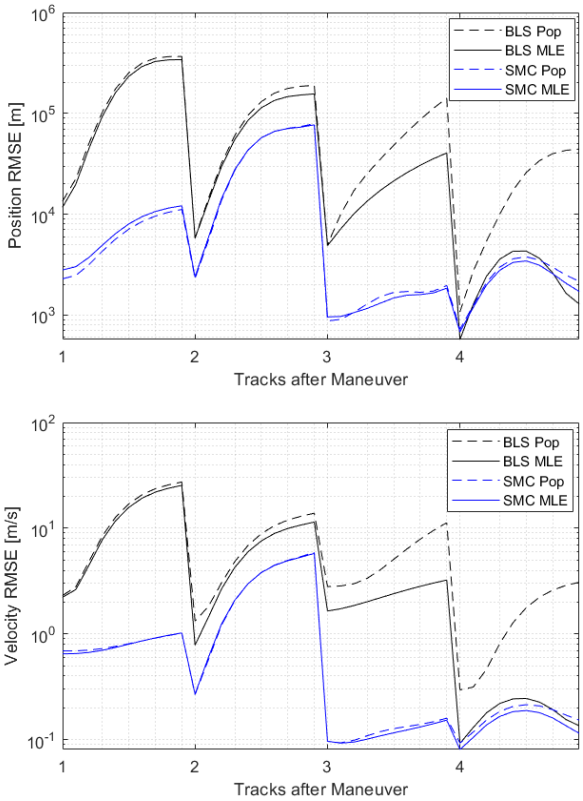

Figure 6: Position (top) and velocity (bottom) Root Mean Square Error (RMSE) as a function of post-maneuver tracks elapsed for the entire state distribution (Pop) and Maximum Likelihood Estimate (MLE).

6.2. Post-maneuver State Estimation

As indicated in the previous section, the majority of errors committed in properly isolating a maneuver are caused by inaccurate post-maneuver state estimates. In the following, the ability of the methods to predict the state of an RSO after performing a maneuver will be evaluated. The metric used in this regard is the Root Mean Squared Error (RMSE) defined as:

$$RMSE_{\mathbf{x}} = \sqrt{\frac{\sum_{i=1}^{n_M}\sum_{j=1}^{n_P}(\mathbf{x}_{i,j}-\hat{\mathbf{x}})^T(\mathbf{x}_{i,j}-\hat{\mathbf{x}})}{n_M n_P}} \tag{17}$$

Where $\mathbf{x}$ represents the velocity or position of the RSO in cartesian coordinates, n_M is the number of maneuvers and n_P is the size of the population under evaluation. Fig. 6 depicts the post-maneuver state estimation (or tracking) performance shown by the batch least squares and sequential monte carlo approaches, note that sudden error drops correspond to measurement updates. Pop refers to the overall root mean square error for the population subset corresponding to the assumed true hypothesis at epoch, whereas MLE stands for the maximum likelihood

estimate of such population subset. A significant reduction in the estimation error is appreciated for both the position and velocity, almost reaching one order of magnitude. In fact, the proposed method is shown to converge to reasonable RMSE values, of the order of 1 km and 0.1 m/s, at the third epoch after the maneuver, while the batch least squares requires at least four tracks after the maneuver to accurately estimate the orbit. Remarkable is the fact that the RMSE for the proposed method between the second and third tracks after the maneuver increases more rapidly than in the interval defined by the first and second post-maneuver tracks. This is caused by the differences in times of flight and thus the implicit dependency on the observation schedule: recall these results are normalized over 22 individual maneuvers

In line with the performances obtained for association and maneuver detection metrics, the proposed method has shown to improve the post-maneuver state characterization when compared to the industry standards. A reduction of almost one order of magnitude in the state estimation error has been found for the simulated test scenario both in terms of position and velocity.

7. CONCLUSIONS AND FUTURE WORK

A novel method for solving the maneuver detection, and implicitly the track association problem, in the context of optical survey scenarios is presented. This method proposes a re-definition of the Admissible Region based on a novel control distance metric considering impulsive burns. Bounds for the maximum expected control effort are given in absolute and relative terms in order to shape the space accessible to an object subject to an optical track in the *Attributable* format. A statistical framework based on this admissible control region is used to characterize the state of a target RSO, relying on the use of Sequential Monte Carlo and Markov Chain Monte Carlo methods. The main filtering and data association tasks are performed via sequential importance sampling and resampling, while post-maneuver state estimation relies on the use of different MCMC algorithms. Depending on the number of tracks available after the maneuver, Metropolis-Hastings or Hamiltonian Monte Carlo schemes are used to sample from the post-maneuver state distribution. Maneuver hypotheses are then generated based on different track association scenarios. Additionally, information derived from already characterized maneuvers can be introduced through conditional sampling, resulting in a feedback loop for the maneuver detection and characterization process. Results are obtained in a simulated test case, representative of an optical survey scenario of a SST sensor framework. Comparison against a Non-Linear Batch Least Squares approach has shown a noticeable improvement in the estimation of the post-maneuver state, thus resulting in enhanced maneuver detection and data association capabilities.

The main contributions of the present work are twofold: on the one hand, a Sequential Monte Carlo filtering framework is successfully applied to the maneuver detection and data association problem; on the other hand, a reformulation of the Admissible Region concept based on a novel control distance metric is proposed to define the space accessible to an object conditioned on an optical track. Direct application of the proposed method may present scalability concerns, especially regarding the computational complexity inherent to SMC methods. The latter may be resolved through a characterization of the state based on Gaussian Mixtures, each representing an individual hypothesis. Samples drawn from MCMC algorithms can then be clustered into additional Gaussian Mixture components. Thereafter, dynamics may be propagated using the Unscented Transform for each individual Gaussian component and measurement update could be based on a Kalman recursion. Still, the capabilities of the proposed method must be evaluated with real measurement data and longer re-observation times.

ACKNOWLEDGEMENTS

This work is part of an ongoing PhD thesis funded by the European Space Agency under the Networking Partnering Initiative through the Project *Combined Heuristic and Statistical Methodologies applied to Maneuver Detection in the SST Observation Correlation Process* and also from "Comunidad de Madrid" under the Project *Métodos avanzados de correlación de medidas y determinación de órbita para la construcción y mantenimiento de un catálogo de objetos espaciales*.

REFERENCES

1. U. S. S. Network, "Satellite box score," *NASA Orbital Debris Quarterly News*, vol. 25, Feb. 2021.
2. D. Escobar, A. Anton, F. Ayuga, A. Pastor, A. Díez, A. Águeda, and J. Lozano, "Methods to build-up and maintain an space objects catalogue," in *1st IAA Conference on Space Situational Awareness (ICSSA)*, Nov. 2017. Nov. 13-15, 2017, Orlando, FL.
3. A. Pastor, D. Escobar, M. Sanjurjo-Rivo, and A. Águeda, "Correlation techniques to build-up and maintain space objects catalogues," in *7th International Conference on Astrodynamics Tools and Techniques*, 2018.
4. A. Pastor, G. Escribano, and D. Escobar, "Satellite maneuver detection with optical survey observations," in *21st Advanced Maui Optical and Space Surveillance Technologies*, 2020.
5. B. Jia, E. Blasch, K. Pham, D. Shen, Z. Wang, X. Tian, and G. Chen, "Space object tracking and maneuver detection via interacting multiple model cubature kalman filters," *IEEE Aerospace Conference Proceedings*, vol. 2015, 06 2015.
6. J. D. Katzovitz, "Space-based maneuver detection and characterization using multiple model adaptive estimation," Master's thesis, 2018.

7. J. Siminski, T. Flohrer, and T. Schildknecht, "Assessment of post-maneuver observation correlation using short-arc tracklets," *Journal of the British Interplanetary Society*, vol. 70, pp. 63–68, 2017.
8. C. Shabarekh, J. Kent-Bryant, G. Keselman, and A. Mitidis, "A novel method for satellite maneuver prediction," in *Advanced Maui Optical and Space Surveillance Technologies Conference.(Maui, Hawaii, USA)*, 2016.
9. M. J. Holzinger, D. J. Scheeres, and K. T. Alfriend, "Object correlation, maneuver detection, and characterization using control distance metrics," *Journal of Guidance, Control, and Dynamics*, vol. 35, no. 4, pp. 1312–1325, 2012.
10. D. P. Lubey, *Maneuver Detection and Reconstruction in Data Sparse Systems with an Optimal Control Based Estimator*. PhD thesis, 2015.
11. R. Serra, C. Yanez, and C. Frueh, "Tracklet-to-orbit association for maneuvering space objects using optimal control theory," *Acta Astronautica*, vol. 181, pp. 271–281, 2021.
12. A. Milani, G. F. Gronchi, M. De' Michieli Vitturi, and Z. Knezevic, "Orbit determination with very short arcs. i - admissible regions," *Celestial Mechanics and Dynamical Astronomy*, vol. 90, pp. 57–85, 07 2004.
13. P. Escobal, *Methods of Orbit Determination*. R. E. Krieger Publishing Company, 1976.
14. A. Milani, G. F. Gronchi, Z. Knežević, M. E. Sansaturio, and O. Arratia, "Orbit determination with very short arcs: Ii. identifications," *Icarus*, vol. 179, no. 2, pp. 350 – 374, 2005.
15. U. D. of Defense, *Joint Doctrine for Space Operations*, 04 2013.
16. K. DeMars, M. Jah, and S. Jr, "Initial orbit determination using short-arc angle and angle rate data," *Aerospace and Electronic Systems, IEEE Transactions on*, vol. 48, pp. 2628–2637, 07 2012.
17. K. DeMars and M. Jah, "Probabilistic initial orbit determination using gaussian mixture models," *Journal of Guidance Control Dynamics*, vol. 36, pp. 1324–1335, 09 2013.
18. T. Kelecy, M. A. Shoemaker, and M. Jah, "Application of the constrained admissible region multiple hypothesis filter to initial orbit determination of a break-up," 2013.
19. J. Stauch, T. Bessell, M. Rutten, J. Baldwin, M. Jah, and K. Hill, "Joint probabilistic data association and smoothing applied to multiple space object tracking," *Journal of Guidance, Control, and Dynamics*, vol. 41, no. 1, pp. 19–33, 2018.
20. L. Pirovano, D. Santeramo, R. Armellin, P. Di Lizia, and A. Wittig, "Probabilistic data association: the orbit set," *Celestial Mechanics and Dynamical Astronomy*, vol. 132, 02 2020.
21. J. Siminski, *Object correlation and orbit determination in the geostationary orbit using optical measurements*. PhD thesis, 01 2016.
22. M. Walker, B. Ireland, and J. Owens, "A set modified equinoctial orbit elements," *Celestial mechanics*, vol. 36, no. 4, pp. 409–419, 1985.
23. D. P. Lubey and D. J. Scheeres, "An optimal control based estimator for maneuver and natural dynamics reconstruction," in *Proceedings of the 2013 Advanced Maui Optical and Space Surveillance Technologies Conference*, 2013.
24. D. P. Lubey and D. J. Scheeres, "Towards real-time maneuver detection: Automatic state and dynamics estimation with the adaptive optimal control based estimator," in *Advanced Maui Optical and Space Surveillance Technologies Conference*, p. 16, 2015.
25. J. A. E. Andersson, J. Gillis, G. Horn, J. B. Rawlings, and M. Diehl, "CasADi – A software framework for nonlinear optimization and optimal control," *Mathematical Programming Computation*, vol. 11, no. 1, pp. 1–36, 2019.
26. T. Nikolayzik, C. Büskens, and M. Gerdts, "Nonlinear large-scale optimization with worhp," in *13th AIAA/ISSMO Multidisciplinary Analysis Optimization Conference*, p. 9136, 2010.
27. A. Wächter and L. T. Biegler, "On the implementation of an interior-point filter line-search algorithm for large-scale nonlinear programming," *Mathematical programming*, vol. 106, no. 1, pp. 25–57, 2006.
28. J. Miguez and A. Artes-Rodriguez, "Monte carlo algorithms for tracking a maneuvering target using a network of mobile sensors," in *1st IEEE International Workshop on Computational Advances in Multi-Sensor Adaptive Processing, 2005.*, pp. 89–92, 2005.
29. N. J. Gordon and A. Doucet, "Sequential Monte Carlo for maneuvering target tracking in clutter," in *Signal and Data Processing of Small Targets 1999* (O. E. Drummond, ed.), vol. 3809, pp. 493 – 500, International Society for Optics and Photonics, SPIE, 1999.
30. W. K. Hastings, "Monte carlo sampling methods using markov chains and their applications," *Biometrika*, vol. 57, no. 1, pp. 97–109, 1970.
31. J. A. Vrugt, "Markov chain monte carlo simulation using the dream software package: Theory, concepts, and matlab implementation," *Environmental Modelling Software*, vol. 75, pp. 273–316, 2016.
32. S. Duane, A. Kennedy, B. J. Pendleton, and D. Roweth, "Hybrid monte carlo," *Physics Letters B*, vol. 195, no. 2, pp. 216–222, 1987.
33. M. D. Hoffman and A. Gelman, "The no-u-turn sampler: Adaptively setting path lengths in hamiltonian monte carlo," 2011.
34. P. C. Mahalanobis, "On the generalised distance in statistics," in *Proceedings of the National Institute of Sciences of India*, vol. 2, pp. 49–55, 1936.
35. J. Maruskin, D. Scheeres, and K. Alfriend, "Correlation of optical observations of objects in earth orbit," *Journal of Guidance, Control, and Dynamics*, vol. 32, 01 2009.

APPENDIX A GAUSS PLANETARY EQUATIONS IN MODIFIED EQUINOCTIAL ELEMENTS

The Gauss Planetary Equations expressed in Modified Equinoctial Elements (MEE) take the form:

$$\frac{dp}{dt} = \frac{2p}{w}\sqrt{\frac{p}{\mu}}a_\theta \tag{18}$$

$$\frac{df}{dt} = \sqrt{\frac{p}{\mu}}\left[\sin(L)a_r + ((w+1)\cos(L)+f)\frac{a_\theta}{w} - (h\sin(L)-k\cos(L))\frac{g}{w}a_h\right] \tag{19}$$

$$\frac{dg}{dt} = \sqrt{\frac{p}{\mu}}\left[-\cos(L)a_r + ((w+1)\sin(L)+g)\frac{a_\theta}{w} + (h\sin(L)-k\cos(L))\frac{f}{w}a_h\right] \tag{20}$$

$$\frac{dh}{dt} = \sqrt{\frac{p}{\mu}}\frac{s^2\cos(L)}{2w}a_h \tag{21}$$

$$\frac{dk}{dt} = \sqrt{\frac{p}{\mu}}\frac{s^2\sin(L)}{2w}a_h \tag{22}$$

$$\frac{dL}{dt} = \sqrt{\mu p}\left(\frac{w}{p}\right)^2 + \frac{1}{w}\sqrt{\frac{p}{\mu}}(h\sin(L)-k\cos(L))a_h \tag{23}$$

where $s^2 = 1+h^2+k^2$ and $w = 1+f\cos(L)+g\sin(L)$. The definition of the MEE in terms of classical orbital elements reads (being ν the true anomaly):

$$p = a(1-e)^2 \tag{24}$$

$$f = e\cos(\omega+\Omega) \tag{25}$$

$$g = e\sin(\omega+\Omega) \tag{26}$$

$$h = \tan(i/2)\cos(\Omega) \tag{27}$$

$$k = \tan(i/2)\sin(\Omega) \tag{28}$$

$$L = \Omega+\omega+\nu \tag{29}$$

APPENDIX B ANALYSIS OF CONTROL DISTANCE METRIC ASSUMPTIONS

Hereunder, the approximation described in Section 4.1 is analyzed for a wide variety of orbits under a nominal maneuver of representative magnitude: $\Delta V_r \equiv \Delta V_\theta \equiv \Delta V_h = 10\ m/s$. The set of initial orbits feature a common semi-major axis $a = 24,000\ km$ and right ascension of the ascending node $\Omega = 0\ deg$, and span the inclination range $i \in [0, 100]\ deg$ and eccentricity range $e \in [10^{-5}, 0.95]$. The entire set $[\omega, \nu] \in [0, 2\pi]$ is considered, but results are given for the maximum error incurred by the linearization, i.e.:

$$\{\omega, \nu\} : \underset{\omega,\nu}{\operatorname{argmax}} \left(||\Delta V - \Delta V_{est}(\text{œ}_0)|| \right)$$

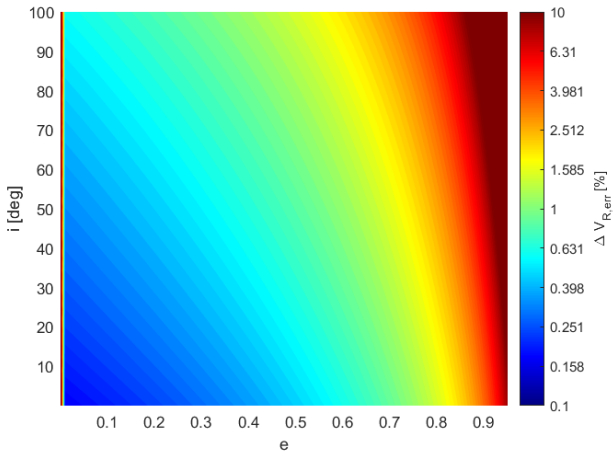

Figure 7: Relative ΔV estimation error for the radial component.

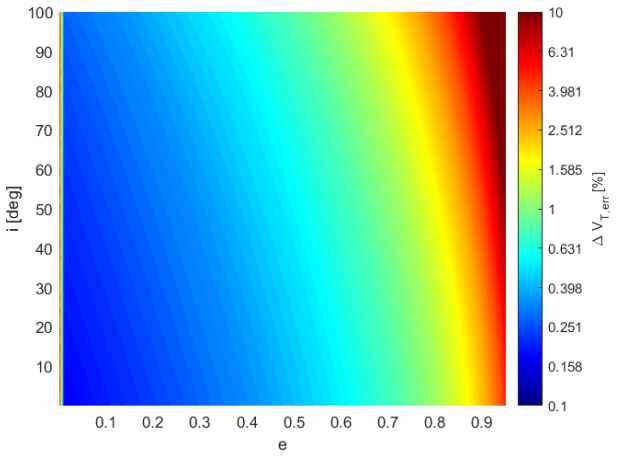

Figure 8: Relative ΔV estimation error for the tangential component.

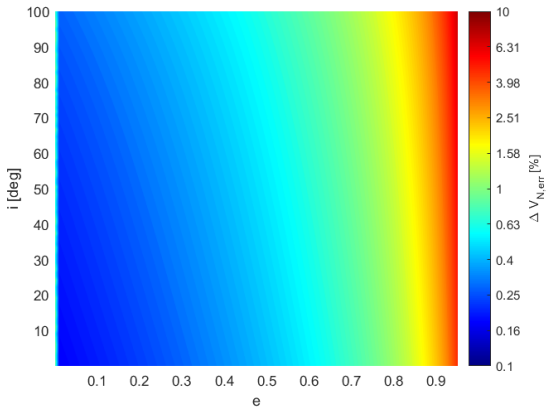

Figure 9: Relative ΔV estimation error for the normal component.